WASHINGTON UNIVERSITY IN ST. LOUIS

REPORT WU/CCM–93/3

Solution of Elastic-Plastic Stress Analysis Problems by the p-Version of the Finite Element Method

Barna A. Szabó, Ricardo L. Actis and
Stefan M. Holzer

November, 1993

Prepared for
Lyndon B. Johnson Space Center
National Aeronautics and
Space Administration
Houston, Texas 77058

CENTER FOR COMPUTATIONAL MECHANICS
WASHINGTON UNIVERSITY
CAMPUS BOX 1129
ST. LOUIS, MO 63130

Center for Computational Mechanics
Washington University
St. Louis, Missouri 63130

Report WU/CCM-93/3

SOLUTION OF ELASTIC-PLASTIC STRESS ANALYSIS PROBLEMS BY THE p-VERSION OF THE FINITE ELEMENT METHOD

Barna A. Szabó
Albert P. and Blanche Y. Greensfelder Professor of Mechanics

Ricardo L. Actis
Senior Research Associate

Stefan M. Holzer
Post-Doctoral Research Fellow

November, 1993

Prepared for:

Lyndon B. Johnson Space Center
National Aeronautics and Space Administration
Houston, TX 77058

TABLE OF CONTENTS

ABSTRACT

The solution of small-strain elastic-plastic stress analysis problems by the p-version of the finite element method is discussed. The formulation is based on the deformation theory of plasticity and the displacement method. Practical realization of controlling discretization errors for elastic-plastic problems is the main focus of the paper. Numerical examples, which include comparisons between the deformation and incremental theories of plasticity under tight control of discretization errors, are presented.

ACKNOWLEDGEMENT

This work has been supported by Lyndon B. Johnson Space Center of the National Aeronautics and Space Administration under Grant NAG 9-622.

KEY WORDS

Plasticity, deformation theory, numerical analysis, finite element method, error estimation.

INTRODUCTION

This paper is concerned with application of the p-version of the finite element method to elastic-plastic stress analysis problems with emphasis on the deformation theory of plasticity. Our interest in this subject is motivated by the following considerations:

(1) The effects of a single overload event on structures made of ductile materials are of substantial practical importance. Such effects can be well represented by mathematical models based on the deformation theory plasticity [1], [2]. This is illustrated by four examples.

(2) The propagation of cracks in strain-hardening materials is generally correlated with the J-integral. The J-integral is based on the deformation theory of plasticity [3], [4].

(3) The p-version is not susceptible to Poisson ratio locking and hence correct limit loads are obtained. In the conventional (h-version) locking occurs when the displacement formulation is is used. For this reason alternative formulations, generally known as mixed methods, must be employed. See, for example, [5]).

(4) Realistic mathematical models of real physical systems must have a capability to provide initial estimates for the effects of nonlinearities at a low computational cost. The deformation theory of plasticity serves this purpose well.

(5) Adaptive control of discretization errors is more important in the case of nonlinear problems than in the case of linear problems because the initial discretization may not be adequate throughout the solution process, hence errors may accumulate in the course of iteration. The p-version, which utilizes hierarchic finite element spaces, is well suited for controlling discretization errors: The number of degrees of freedom can be increased substantially without mesh refinement. It is particularly advantageous to use adaptive p-distributions in nonlinear cycles because the gains in performance, as compared with unadapted schemes, are multiplied by the number of iteration steps.

(6) From the point of view of implementation, the data storage requirements for the deformation theory are much smaller than for the incremental theory.

The p-version of the finite element method became well established during the 1980's. Its theoretical basis is now thoroughly developed and its performance characteristics are extensively documented. We refer to [6] and the references listed therein. With the exception of adaptive hp-extensions in fluid dynamics (see, for example, [7]), virtually all documented applications of the p-version have been to linear problems, and particularly to problems belonging to the following two categories:

Category A: The exact solution is analytic on the entire solution domain and its boundaries.

Category B: The exact solution is analytic on the entire solution domain and its boundaries, with the exception of a finite number of points (in three dimensions finite number of points and lines). The points where the solution is not analytic are called singular points.

The p-version is effective for problems in Categories A and B because exponential convergence rates can be achieved, within the range of accuracy normally expected in engineering practice, with simple finite element meshes.

The effectiveness of the p-version depends on the smoothness of the underlying exact solution $\vec{u}_{EX}$ and the design of the finite element mesh with respect to $\vec{u}_{EX}$. Certain types of nonlinearities, such as material nonlinearities associated with nonlinear elasticity and the deformation theory of plasticity, and even a broad class of problems solved by the incremental theory of plasticity, do not perturb the smoothness of the underlying exact solution significantly. Therefore the p-version is an effective method for solving such problems. In fact, the performance characteristics of the p-version can be expected to be substantially the same as in the case of linear problems belonging in categories A and B. This expected behavior has been confirmed with respect to a set of benchmark problems, four of which are presented in this paper.

The assumptions on which the deformation theory of plasticity is based; the elastic-plastic compliance matrices for the cases of plane stress, plane strain and axisymmetric problems; an outline of the algorithmic procedure and examples are presented in this paper.

FORMULATION OF THE MATHEMATICAL PROBLEM

The cases of plane stress, plane strain and axially symmetric problems, that is, two-dimensional formulations, are considered in the following. The formulations are based on the displacement method.

Notation.

The components of the displacement vector $\vec{u}$ are denoted by $u_x = u_x(x,y)$ and $u_y = u_y(x,y)$ The components of the small strain tensor, by definition, are:

$$\epsilon_x \stackrel{\text{def}}{=} \frac{\partial u_x}{\partial x} \tag{1a}$$

$$\epsilon_y \stackrel{\text{def}}{=} \frac{\partial u_y}{\partial y} \tag{1b}$$

$$\epsilon_z \stackrel{\text{def}}{=} \frac{\partial u_z}{\partial z} \tag{1c}$$

$$\epsilon_{xy} \stackrel{\text{def}}{=} \frac{1}{2}\left(\frac{\partial u_x}{\partial y} + \frac{\partial u_y}{\partial x}\right). \tag{1d}$$

In addition, $\gamma_{xy} \stackrel{\text{def}}{=} 2\epsilon_{xy}$ will be used to represent the usual engineering definition of strain. The elastic (resp. plastic) strains will be indicated by the superscript e (resp. p). The three principal strains are denoted by ϵ_1, ϵ_2, ϵ_3. The equivalent elastic strain is defined by:

$$\bar{\epsilon}^e \stackrel{\text{def}}{=} \frac{\sqrt{2}}{2(1+\nu)}\sqrt{(\epsilon_1^e - \epsilon_2^e)^2 + (\epsilon_2^e - \epsilon_3^e)^2 + (\epsilon_3^e - \epsilon_1^e)^2} \tag{2a}$$

where ν is Poisson's ratio. The equivalent plastic strain is defined by

$$\bar{\epsilon}^p \stackrel{\text{def}}{=} \frac{\sqrt{2}}{3}\sqrt{(\epsilon_1^p - \epsilon_2^p)^2 + (\epsilon_2^p - \epsilon_3^p)^2 + (\epsilon_3^p - \epsilon_1^p)^2} \tag{2b}$$

and the total equivalent strain is, by definition,

$$\bar{\epsilon} \stackrel{\text{def}}{=} \bar{\epsilon}^e + \bar{\epsilon}^p. \tag{2c}$$

The uniaxial strain at the onset of yielding is denoted by ϵ_Y.

The stress tensor components are denoted by σ_x, σ_y, σ_z, τ_{xy}. The three principal stress components are denoted by σ_1, σ_2, σ_3. The equivalent stress is defined by:

$$\bar{\sigma} \stackrel{\text{def}}{=} \frac{\sqrt{2}}{2}\sqrt{(\sigma_1 - \sigma_2)^2 + (\sigma_2 - \sigma_3)^2 + (\sigma_3 - \sigma_1)^2} \tag{3}$$

The components of the stress deviator tensor are denoted by $\tilde{\sigma}_x$, $\tilde{\sigma}_y$, $\tilde{\sigma}_z$, $\tilde{\tau}_{xy}$. By definition,

$$\tilde{\sigma}_x = \sigma_x - \frac{1}{3}(\sigma_x + \sigma_y + \sigma_z) \tag{4a}$$

$$\tilde{\sigma}_y = \sigma_y - \frac{1}{3}(\sigma_x + \sigma_y + \sigma_z) \tag{4b}$$

$$\tilde{\sigma}_z = \sigma_z - \frac{1}{3}(\sigma_x + \sigma_y + \sigma_z) \tag{4c}$$

$$\tilde{\tau}_{xy} = \tau_{xy} \tag{4d}$$

The second invariant of the stress deviator tensor is denoted by J_2 and is defined by:

$$J_2 \stackrel{\text{def}}{=} \frac{1}{2}(\tilde{\sigma}_x^2 + \tilde{\sigma}_y^2 + \tilde{\sigma}_z^2) + \tilde{\tau}_{xy}^2. \tag{5}$$

In the case of axial symmetry the independent variables are denoted by r, θ, z instead of x, y, z. In the one-dimensional case (i.e., uniaxial stress state) the subscripts are omitted.

Assumptions.

The assumptions on which the formulation of the mathematical problem is based are described in the following.

Assumption 1:

The strain components are much smaller than unity on the solution domain and its boundary, and the deformations are small in the sense that equilibrium equations written for the undeformed configuration are essentially the same as the equilibrium equations written for the deformed configuration.

Assumption 2:

The total strain is the sum of the elastic strain and the plastic strain.

Referring to Fig. 1, in the case of uniaxial stress state the stress-strain law is:

$$\epsilon^e + \epsilon^p = \frac{\sigma}{E_s}$$

where E_s is the secant modulus. Since the elastic part of the strain is related to the stress by Hooke's law:

$$\epsilon^e = \frac{\sigma}{E}$$

where E is the modulus of elasticity, we have:

$$\epsilon^p = \left(\frac{1}{E_s} - \frac{1}{E}\right)\sigma. \tag{6}$$

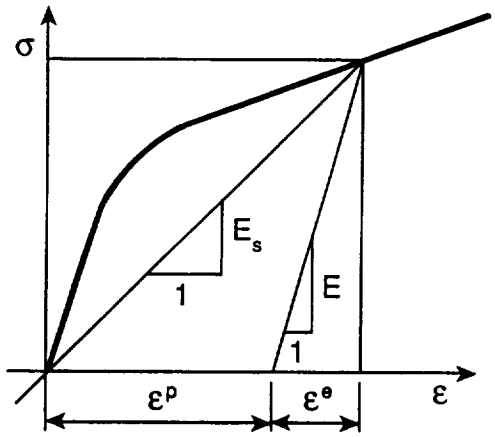

Fig. 1. Typical uniaxial stress-strain curve.

Assumption 3:

The absolute values of the stress tensor components are non-decreasing and the stress tensor components remain in a fixed proportion as the deformation progresses.

Assumption 4:

The plastic strain tensor is proportional to the stress deviator tensor.

Assumptions 3 and 4 allow generalization of the uniaxial stress state for which experimental information is available to two and three dimensions. In the case of uniaxial stress state $\tilde{\sigma} = 2\sigma/3$ and hence eq. (6) can be written as:

$$\epsilon^p = \frac{3}{2}\left(\frac{1}{E_S} - \frac{1}{E}\right)\tilde{\sigma}. \tag{7a}$$

In two-dimensional problems:

$$\begin{Bmatrix} \epsilon_x^p \\ \epsilon_y^p \\ \epsilon_z^p \\ \epsilon_{xy}^p \end{Bmatrix} = \frac{3}{2}\left(\frac{1}{E_s} - \frac{1}{E}\right)\begin{Bmatrix} \tilde{\sigma}_x \\ \tilde{\sigma}_y \\ \tilde{\sigma}_z \\ \tilde{\tau}_{xy} \end{Bmatrix}. \tag{7b}$$

Remark:

In the incremental theory of plasticity based on the von Mises yield criterion the following assumption, analogous to Assumption 4, is made: Increments of the tensor components of the plastic strain are proportional to the first derivatives of J_2 with respect to the corresponding components of the stress tensor. The first derivatives of J_2 with respect σ_x, σ_y, σ_z and τ_{xy} can be shown to be equal to $\tilde{\sigma}_x$, $\tilde{\sigma}_y$, $\tilde{\sigma}_z$ and $\tilde{\tau}_{xy}$, respectively. Thus, for example;

$$d\epsilon_x^p = d\lambda \frac{\partial J_2}{\partial \sigma_x} = d\lambda\, \tilde{\sigma}_x.$$

In the one-dimensional case:

$$d\epsilon^p = d\bar{\epsilon}^p = d\lambda\, \tilde{\sigma} = \frac{2}{3} d\lambda\, \bar{\sigma}$$

hence:

$$d\epsilon_x^p = \frac{3}{2} \frac{d\bar{\epsilon}^p}{\bar{\sigma}} \tilde{\sigma}_x. \tag{8}$$

Analogous relationships hold for the plastic increments of each component of the strain tensor.

The elastic-plastic material compliance matrix in the case of plane stress.

Using the definition of the stress deviator, given by (3), and the relationship between the plastic strain and deviatoric stress (7b), we have:

$$\begin{Bmatrix} \epsilon_x^p \\ \epsilon_y^p \\ \gamma_{xy}^p \end{Bmatrix} = \frac{3}{2}\left(\frac{1}{E_s} - \frac{1}{E}\right) \begin{bmatrix} 2/3 & -1/3 & 0 \\ -1/3 & 2/3 & 0 \\ 0 & 0 & 2 \end{bmatrix} \begin{Bmatrix} \sigma_x \\ \sigma_y \\ \tau_{xy} \end{Bmatrix}.$$

Using $\{\epsilon\} = \{\epsilon^e\} + \{\epsilon^p\}$ a relationship is obtained between the total strain components and the stress tensor:

$$\begin{Bmatrix} \epsilon_x \\ \epsilon_y \\ \gamma_{xy} \end{Bmatrix} = \left(\frac{1}{E} \begin{bmatrix} 1 & -\nu & 0 \\ -\nu & 1 & 0 \\ 0 & 0 & 2(1+\nu) \end{bmatrix} + \frac{E - E_s}{E_s E} \begin{bmatrix} 1 & -1/2 & 0 \\ -1/2 & 1 & 0 \\ 0 & 0 & 3 \end{bmatrix} \right) \begin{Bmatrix} \sigma_x \\ \sigma_y \\ \tau_{xy} \end{Bmatrix}. \tag{9a}$$

The matrix in the brackets is the elastic-plastic material compliance matrix which is readily invertible to obtain the material stiffness matrix.

Remark:

Referring to Fig. 1 and the definitions for the equivalent plastic strain and equivalent stress, it can be easily shown that

$$\frac{(E-E_s)}{EE_s} = \frac{\epsilon^p}{\sigma} = \frac{\bar{\epsilon}^p}{\bar{\sigma}}.$$

In view of Eq. (8), in the incremental theory of plasticity the equation analogous to (9a) is:

$$\begin{Bmatrix} d\epsilon_x \\ d\epsilon_y \\ d\gamma_{xy} \end{Bmatrix} = \frac{1}{E}\begin{bmatrix} 1 & -\nu & 0 \\ -\nu & 1 & 0 \\ 0 & 0 & 2(1+\nu) \end{bmatrix} \begin{Bmatrix} d\sigma_x \\ d\sigma_y \\ d\tau_{xy} \end{Bmatrix} + \frac{d\bar{\epsilon}^p}{\bar{\sigma}} \begin{bmatrix} 1 & -1/2 & 0 \\ -1/2 & 1 & 0 \\ 0 & 0 & 3 \end{bmatrix} \begin{Bmatrix} \sigma_x \\ \sigma_y \\ \tau_{xy} \end{Bmatrix}. \qquad (9b)$$

The elastic-plastic material compliance matrix in the case of plane strain.

In the case of plane strain we have

$$\epsilon_z = \epsilon_z^e + \epsilon_z^p = 0$$

where

$$\epsilon_z^e = \frac{1}{E}(\sigma_z - \nu\sigma_x - \nu\sigma_y)$$

$$\epsilon_z^p = \frac{3}{2}\left(\frac{1}{E_s} - \frac{1}{E}\right)\tilde{\sigma}_z = \frac{3}{2}\left(\frac{1}{E_s} - \frac{1}{E}\right)\left(\frac{2}{3}\sigma_z - \frac{1}{3}\sigma_x - \frac{1}{3}\sigma_y\right).$$

Therefore:

$$\sigma_z = \frac{1}{2}\left[1 - \frac{E_s}{E}(1-2\nu)\right](\sigma_x + \sigma_y)$$

and

$$\begin{aligned}\tilde{\sigma}_x &= \sigma_x - \frac{1}{3}(\sigma_x + \sigma_y + \sigma_z) \\ &= \sigma_x - \frac{1}{3}\left(\sigma_x + \sigma_y + \frac{1}{2}\left[1 - \frac{E_s}{E}(1-2\nu)\right](\sigma_x + \sigma_y)\right) \\ &= \left[\frac{1}{2} + \frac{1}{6}\frac{E_s}{E}(1-2\nu)\right]\sigma_x - \left[\frac{1}{2} - \frac{1}{6}\frac{E_s}{E}(1-2\nu)\right]\sigma_y.\end{aligned}$$

Similarly:

$$\tilde{\sigma}_y = -\left[\frac{1}{2} - \frac{1}{6}\frac{E_s}{E}(1-2\nu)\right]\sigma_x + \left[\frac{1}{2} + \frac{1}{6}\frac{E_s}{E}(1-2\nu)\right]\sigma_y.$$

The elastic strain components in terms of the stress components are:

$$\epsilon_x^e = \frac{1}{E}\left(1 - \frac{\nu}{2} + \frac{\nu}{2}\frac{E_s}{E}(1-2\nu)\right)\sigma_x - \frac{\nu}{E}\left(\frac{3}{2} - \frac{E_s}{2E}(1-2\nu)\right)\sigma_y \tag{10a}$$

$$\epsilon_y^e = -\frac{\nu}{E}\left(\frac{3}{2} - \frac{E_s}{2E}(1-2\nu)\right)\sigma_x + \frac{1}{E}\left(1 - \frac{\nu}{2} + \frac{\nu}{2}\frac{E_s}{E}(1-2\nu)\right)\sigma_y \tag{10b}$$

$$\gamma_{xy}^e = \frac{2(1+\nu)}{E}\tau_{xy} \tag{10c}$$

and the plastic strain components in terms of the stress components are:

$$\epsilon_x^p = \frac{E-E_s}{E_sE}\left[\frac{3}{4} + \frac{1}{4}\frac{E_s}{E}(1-2\nu)\right]\sigma_x - \frac{E-E_s}{E_sE}\left[\frac{3}{4} - \frac{1}{4}\frac{E_s}{E}(1-2\nu)\right]\sigma_y \tag{11a}$$

$$\epsilon_y^p = -\frac{E-E_s}{E_sE}\left[\frac{3}{4} - \frac{1}{4}\frac{E_s}{E}(1-2\nu)\right]\sigma_x + \frac{E-E_s}{E_sE}\left[\frac{3}{4} + \frac{1}{4}\frac{E_s}{E}(1-2\nu)\right]\sigma_y \tag{11b}$$

$$\gamma_{xy}^p = 3\frac{E-E_s}{E_sE}\tau_{xy}. \tag{11c}$$

Combining equations (10a,b,c) and (11a,b,c), the elastic-plastic material compliance matrix can be written in the form:

$$[C] \stackrel{\text{def}}{=} \begin{bmatrix} C_{11} & C_{12} & 0 \\ C_{12} & C_{11} & 0 \\ 0 & 0 & C_{33} \end{bmatrix}$$

where:

$$C_{11} = \frac{1}{E}\left(1 - \frac{\nu}{2} + \frac{\nu}{2}\frac{E_s}{E}(1-2\nu)\right) + \frac{E-E_s}{EE_s}\left[\frac{3}{4} + \frac{1}{4}\frac{E_s}{E}(1-2\nu)\right]$$

$$C_{12} = -\frac{\nu}{E}\left(\frac{3}{2} - \frac{E_s}{2E}(1-2\nu)\right) - \frac{E-E_s}{EE_s}\left[\frac{3}{4} - \frac{1}{4}\frac{E_s}{E}(1-2\nu)\right]$$

$$C_{33} = \frac{2(1+\nu)}{E} + 3\frac{E-E_s}{EE_s}.$$

To obtain the elastic-plastic material stiffness matrix, $[C]$ is inverted.

The elastic-plastic material compliance matrix in the case of axial symmetry.

In the axisymmetric case the elastic part of the the radial, circumferential and axial strain components are related to the corresponding stress components by Hooke's law:

$$\epsilon_r^e = \frac{1}{E}\left(\sigma_r - \nu\sigma_\theta - \nu\sigma_z\right)$$

$$\epsilon_\theta^e = \frac{1}{E}\left(-\nu\sigma_r + \sigma_\theta - \nu\sigma_z\right)$$

$$\epsilon_z^e = \frac{1}{E}\left(-\nu\sigma_r - \nu\sigma_\theta + \sigma_z\right).$$

The plastic strain components are related to the stress by:

$$\begin{Bmatrix} \epsilon_r^p \\ \epsilon_\theta^p \\ \epsilon_z^p \end{Bmatrix} = \frac{3}{2}\left(\frac{1}{E_s} - \frac{1}{E}\right)\begin{bmatrix} 2/3 & -1/3 & -1/3 \\ -1/3 & 2/3 & -1/3 \\ -1/3 & -1/3 & 2/3 \end{bmatrix}\begin{Bmatrix} \sigma_r \\ \sigma_\theta \\ \sigma_z \end{Bmatrix}.$$

The elastic-plastic compliance matrix is of the form:

$$[C] \stackrel{\text{def}}{=} \begin{bmatrix} C_{11} & C_{12} & C_{12} & 0 \\ C_{12} & C_{11} & C_{12} & 0 \\ C_{12} & C_{12} & C_{11} & 0 \\ 0 & 0 & 0 & C_{44} \end{bmatrix}$$

where:

$$C_{11} = \frac{1}{E_s}, \quad C_{12} = -\frac{1}{2EE_s}(E - E_s(1-2\nu)), \quad C_{44} = \frac{2(1+\nu)}{E} + 3\frac{E - E_s}{EE_s}.$$

Since the elastic-plastic compliance matrix has a special structure, its inverse can be readily computed to obtain the elastic-plastic stiffness matrix.

OUTLINE OF THE SOLUTION ALGORITHM

Following is an outline of the procedure used in solving the elastic-plastic problems based on the deformation theory of plasticity described in the next section. The procedure is known as direct iteration. The iteration number is represented by a superscript in brackets.

1. Obtain a linear solution. Ensure that the relative error in energy norm is small, certainly under 5 percent, preferably under 1 percent. It is good practice to check the quality of the discretization by observing or computing the degree of continuity in the stress field.
2. Compute the equivalent elastic strain $\bar{\varepsilon}^e$ in each Gauss point and let $(\bar{\varepsilon})^{(1)} = (\bar{\varepsilon}^e)^{(1)}$.
3. Using $(\bar{\varepsilon})^{(k)}$, compute the secant modulus $E_s^{(k)}$ corresponding to each Gauss point from the one-dimensional stress-strain curve.
4. In each Gauss point for which $\bar{\varepsilon} > \epsilon_Y$ determine the elastic-plastic material stiffness matrix. Recompute the stiffness matrices for those elements for which $\bar{\varepsilon} > \epsilon_Y$ in one or more Gauss points, and obtain a new finite element solution $\vec{u}_{FE}^{(k+1)}$.
5. Using $E_s^{(k)}$ and $\vec{u}_{FE}^{(k+1)}$, compute the stress tensor components $\{\sigma^{(k+1)}\}$ in each Gauss point, using the total strain computed from $\vec{u}_{FE}^{(k+1)}$ and the elastic-plastic material stiffness matrix. Determine the elastic strains from $\{\sigma^{(k+1)}\}$ and the elastic part of the material stiffness matrix, i.e., Hooke's law. Compute the plastic strain by subtracting the elastic strain components from the corresponding total strain components.
6. Compute equivalent strains $(\bar{\varepsilon}^e)^{(k+1)}$, $(\bar{\varepsilon}^p)^{(k+1)}$ and $\bar{\varepsilon}^{(k+1)}$ from (2.a,b,c). If in each Gauss point the following criterion is met:

$$\frac{|\bar{\varepsilon}^{(k+1)} - \bar{\varepsilon}^{(k)}|}{\bar{\varepsilon}^{(k+1)}} \leq \tau_\epsilon \tag{12}$$

where τ_ϵ is a pre-specified tolerance, then stop, else using $\bar{\varepsilon}^{(k+1)}$, compute $E_s^{(k+1)}$, increment $k \rightarrow k+1$ and return to step 3.

EXAMPLES

The solutions of representative examples are solved in the following. Results obtained by application of the deformation theory and numerical solution by the p-version are compared with results obtained by applications of the incremental theory of plasticity and solutions obtained h- and p-extensions.

The boundary conditions are described in terms of the normal (resp. tangential) displacement vector component u_n (resp. u_t) and the normal (resp. tangential) traction vector component T_n (resp. T_t).

Example 1: Plane Strain.

In this example differences in computed data attributable to alternative elastic-plastic models are examined under tight control of the discretization errors. Two models of elastic-plastic material response are compared: Model 1 is based on the deformation theory of plasticity and the von Mises yield criterion, implemented as described in this paper. The numerical solution was obtained by the finite element analysis program PEGASYS†. Model 2 is based on the incremental theory of plasticity and the von Mises yield criterion. The numerical solution for Model 2 was obtained by an experimental computer program, called FEASIBLE [8]. Both programs have p-extension capabilities.

The solution domain and finite element mesh are shown in Figure 2. Along AB and DE symmetry boundary conditions are applied, that is, $u_n = T_t = 0$. Along BC $T_n = 24$, $T_t = 0$. Along CD $T_n = 30$, $T_t = 0$ and along EA $T_n = T_t = 0$.

The material is assumed to be elastic-perfectly plastic. Therefore three parameters characterize the stress-strain relationship: The modulus of elasticity (E) is 1000, Poisson's ratio (ν) is 0.3 the yield stress (σ_Y) is 20. The thickness is unity.

The numerical solutions were obtained by the p-version of the finite element method using the six-element mesh shown in Fig. 2 and the product space. The product space of degree p is the span of the set of monomials $\xi^i\eta^j$, $i,j = 0,1,2,\ldots,p$ on the standard quadrilateral element ($|\xi| \leq 1$, $|\eta| \leq 1$). For both models the number of Gaussian quadrature points was fixed at 14×14 for all p-levels.

† *PEGASYS is a trademark of Engineering Software Research and Development, Inc., 7750 Clayton Road, St. Louis, MO 63117.*

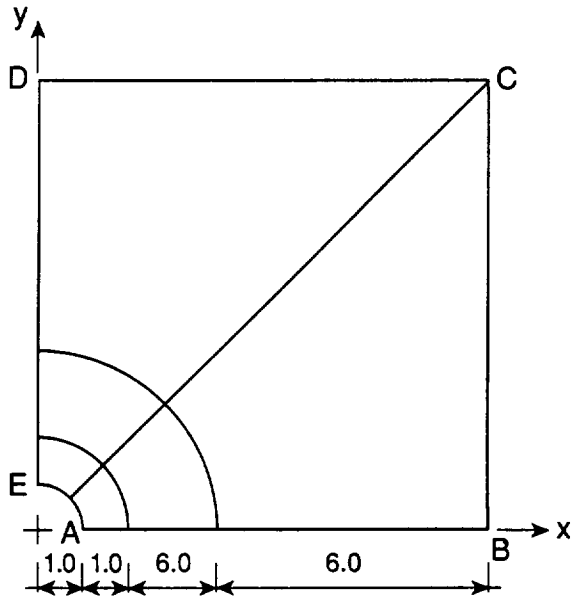

Fig. 2. Solution domain and 6-element mesh for Model 1.

The number of degrees of freedom (N), the potential energy computed from the finite element solutions (Π_{FE}) and the estimated relative error in energy norm are given in Table 1 for the linear solution. It is seen that the numerical error at $p = 8$ is less than 0.01 percent.

Table 1. Estimated relative error in energy norm for the linear solution.

p	N	Π_{FE}	$(e_r)_E$ (%)
1	16	−39.9521346350	7.13
2	56	−40.1432844703	1.80
3	120	−40.1554486036	0.44
4	208	−40.1561743285	0.12
5	320	−40.1562305887	0.03
6	456	−40.1562347043	0.01
7	616	−40.1562350709	0.00
8	800	−40.1562351098	0.00
∞	∞	−40.1562351165	0.00

The tolerances for the errors in the iterative solutions were set so small that the approximation errors can be considered negligible. Therefore the results show variations due to the alternative mathematical models of elastic-plastic material behavior. In Model 1 $\tau_\epsilon = 0.001$ was used (see eq. (12)). In Model 2 the error

tolerance was set on the residuals in the equilibrium iteration. Specifically, the tolerance was $\sqrt{(\delta r)^T \delta r / r^T r} \leq 1.0^{-4}$ where $\delta r \stackrel{\text{def}}{=} [\delta K]x - r$, $[\delta K]$ is the change in stiffness matrix after the current iteration, x is the current solution vector and r is the current load vector.

Table 2. Circumferential strain (ϵ_t)
at the perimeter of the circular hole. Product space, p=8.

θ degrees	Model 1	Model 2	Relative diff. (%)
0	0.1340	0.1318	+1.7
22.5	0.1272	0.1248	+1.9
45	0.1029	0.0989	+4.0
67.5	0.0604	0.0576	+4.9
90	0.0354	0.0362	−2.2

Models 1 and 2 are compared on the basis of the circumferential strain (ϵ_t) along the perimeter of the circular hole. By definition:

$$\epsilon_t \stackrel{\text{def}}{=} \frac{\epsilon_x + \epsilon_y}{2} - \frac{\epsilon_x - \epsilon_y}{2} \cos 2\theta - \frac{\gamma_{xy}}{2} \sin 2\theta$$

where θ is the angle measured from the positive x-axis. The results are listed in Table 2. The results for Model 2 were used for reference. in computing the relative differences shown in Table 2. It is seen that the differences between the deformation and incremental theories of plasticity are not greater than the errors in physical experiments on the basis of which alternative yield criteria are tested and the requisite material properties are determined.

Table 3. p-Convergence of the circumferential strain (ϵ_t)
at the perimeter of the circular hole. Model 1, product space.

p	N	$\theta = 0$	$\theta = 22.5°$	$\theta = 45°$	$\theta = 67.5°$	$\theta = 90°$
2	56	0.1383	0.1112	0.0927	0.0610	0.0407
3	120	0.1346	0.1258	0.1013	0.0593	0.0372
4	208	0.1329	0.1268	0.1004	0.0606	0.0372
5	320	0.1340	0.1269	0.1012	0.0604	0.0366

Control of the discretization errors by p-extension was found to be very effective. Letting $\tau_\epsilon = 0.01$, and using the default values for the number of quadrature points, which are p-dependent, it was possible to obtain substantially the same results as in the case of the extremely tight control of discretization and iteration errors described above. The results are shown in Table 3.

A similar problem was solved by Galin using classical methods [7], [8]. Galin considered a circular opening in an infinite elastic-perfectly plastic medium, subjected to uniform stresses at infinity. Galin's solution is based on the Tresca yield criterion. Because there are differences in the boundary conditions, as compared with Models 1 and 2, strict comparison between Galin's solutions and the solutions presented herein is not possible. Nevertheless, because the domain is much larger than the circular opening, the differences caused by the differences in boundary conditions are very likely to be minor and therefore differences in the solution are caused primarily by the differences in the von Mises and Tresca yield conditions. The contour lines which separate the yielded and unyielded materials for the Galin solution and Models 1 and 2 are shown in Fig. 3. For Galin's problem this contour is an ellipse with major axis of $3.05/r_0$, $1.64/r_0$ where r_0 is the radius of the circular hole.

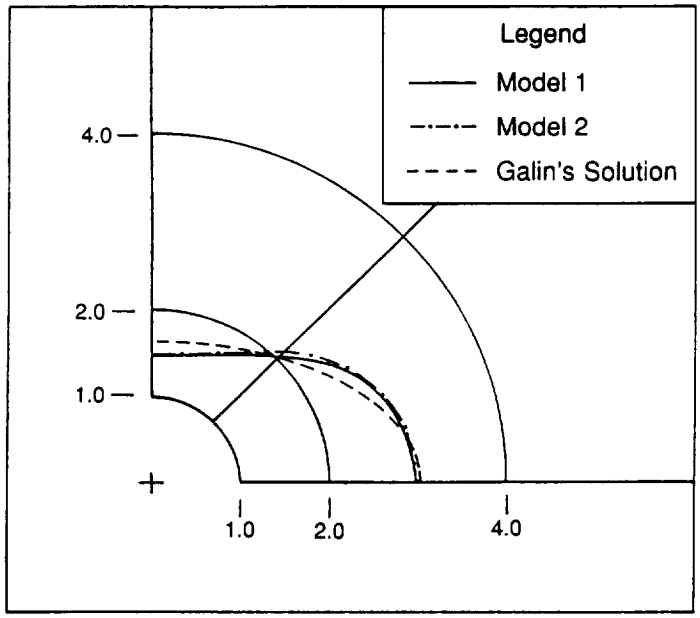

Fig. 3. Contours separating the yielded and unyielded regions.

Example 2: Plane Stress.

In this problem we consider the elastic-plastic response of a thin perforated strip of a strain-hardening material to loading by enforced displacements. The results of the numerical analysis are compared with those obtained experimentally by Theocaris and Marketos in [11].

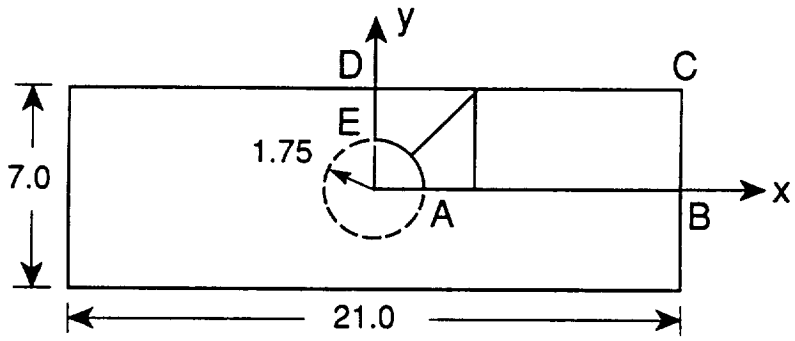

Fig. 4. Perforated strip. Notation.

The strip is shown in Fig. 4. All dimensions are in inch units. Taking advantage of symmetry, the solution domain was one fourth of the strip which was discretized using three finite elements, as shown in Fig. 4. Along AB and DE symmetry boundary conditions were prescribed ($u_n = T_t = 0$); along BC normal displacement (Δ) was imposed ($u_n = \Delta$, $T_t = 0$); along CD and EA the boundary was stress free ($T_n = T_t = 0$).

The material properties are typical of an aluminum alloy with yield strength in tension $\sigma_Y = 34,500$ psi, and ultimate strength $\sigma_{UTS} = 40,000$ psi. The modulus of elasticity is $E = 9.956 \times 10^6$ psi, Poisson's ratio $\nu = 0.30$, and the plastic tangent modulus $E_t = 3.2 \times 10^5$ psi. Plane stress conditions were assumed.

The stress-strain curve in uniaxial tension, shown in Fig. 5, was characterized by five parameters: The slope of the linear part (E), the slope of the constant strain-hardening part (E_t), the stress at the end of the linear slope ($\sigma_1 = 26,000$ psi), and the smallest values of stress ($\sigma_2 = 35,500$ psi) and strain ($\epsilon_2 = 0.0055$) corresponding to E_t.

For each value of the imposed displacement (Δ), the resultant force F along the edge of the strip and the maximum strain ϵ_x at the point of first yield (which occurs

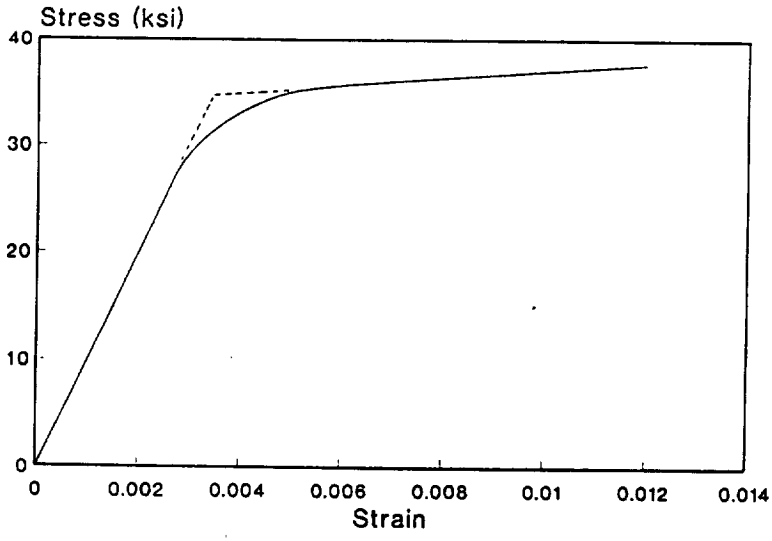

Fig. 5. Example 2: Stress-strain curve in tension based on five parameters.

at the edge of the hole) were computed from the finite element solution obtained for polynomial degree 8 using the trunk space (also known as the 'serendipity' space). The trunk space of degree p is defined on the standard quadrilateral element ($|\xi| \leq 1$, $|\eta| \leq 1$) as the span of the set of monomials $\xi^i \eta^j$, $i, j = 0, 1, 2, \ldots, p$, $i + j \leq p$, augmented by the monomials $\xi^p \eta$, $\xi \eta^p$ for $p \geq 2$ and by the monomial $\xi \eta$ for $p = 1$.

The number of degrees of freedom was 211. The estimated relative error in energy norm of the starting (linear) solution was 0.23 percent The stopping criterion for the nonlinear solution was set at $r_\epsilon = 0.001$ (see eq. (12)).

Table 4. Results for the perforated strip shown in Fig. 4.

Δ (in)	σ_{AV}/σ_Y	$E\epsilon_z/\sigma_Y$
0.0050	0.217	0.469
0.0100	0.433	0.948
0.0125	0.541	1.251
0.0150	0.645	1.686
0.0175	0.744	2.188
0.0200	0.836	2.659
0.0225	0.917	3.273
0.0250	0.981	4.064
0.0275	1.027	5.269
0.0300	1.055	6.862

The results of the analysis for various values of the imposed displacement are

presented in Table 4 and in Fig. 6. Figure 6 also includes the experimental results which were extracted by reading the values from the plots provided in [10]. The normalized stress, σ_{AV}/σ_Y, is defined as the ratio between the average stress and the yield strength:

$$\frac{\sigma_{AV}}{\sigma_Y} = \frac{F}{A_{\min}\sigma_Y}$$

and the normalized strain is defined as the ratio between the strain ϵ_z and the yield strain (σ_Y/E). The plastic region is confined up to the maximum normalized strain reaching a value of approximately 4.0.

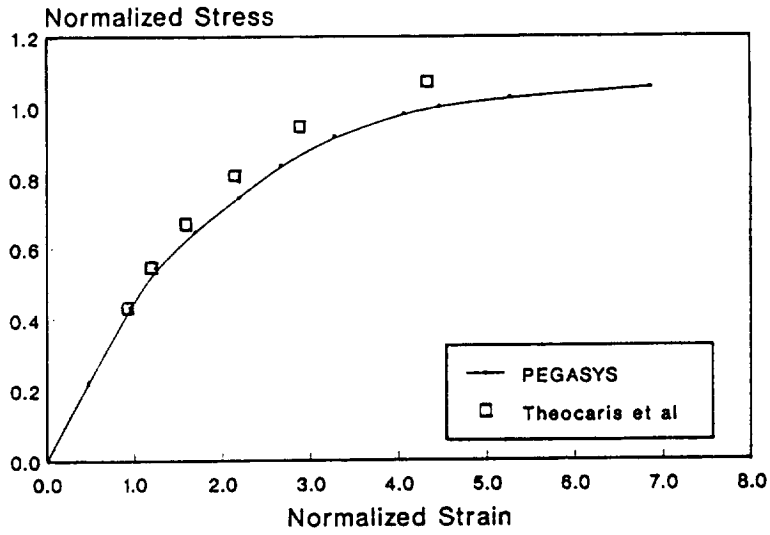

Fig. 6. Perforated strip: Average stress vs. Maximal normalized strain

It is seen in Fig. 6 that the computed strain is larger than the experimentally observed strain. Other investigators reported similar discrepancies. A possible explanation is that in the case of the numerical solution the strain is reported with an infinitesimal gauge length wheres experimentally determined strains invariably involve some gauge length of finite size.

Example 3: An axisymmetric problem.

In this problem we consider the elastic-plastic behaviour of a thin-walled spherical pressure vessel with a cylindrical nozzle under uniform internal pressure. The results of the analysis for an elastic - perfectly plastic material are compared

with those obtained experimentally by Dinno and Gill in [12], and numerically by Zienkiewicz in [13].

The generating section and the finite element mesh, consisting of 14 elements, are shown in Fig. 7. All dimensions are in inch units. The material properties are typical of a steel alloy with yield strength in tension $\sigma_Y = 40,540$ psi, modulus of elasticity $E = 29.12 \times 10^6$ psi, Poisson's ratio $\nu = 0.30$, and zero strain hardening $(E_t = 0)$.

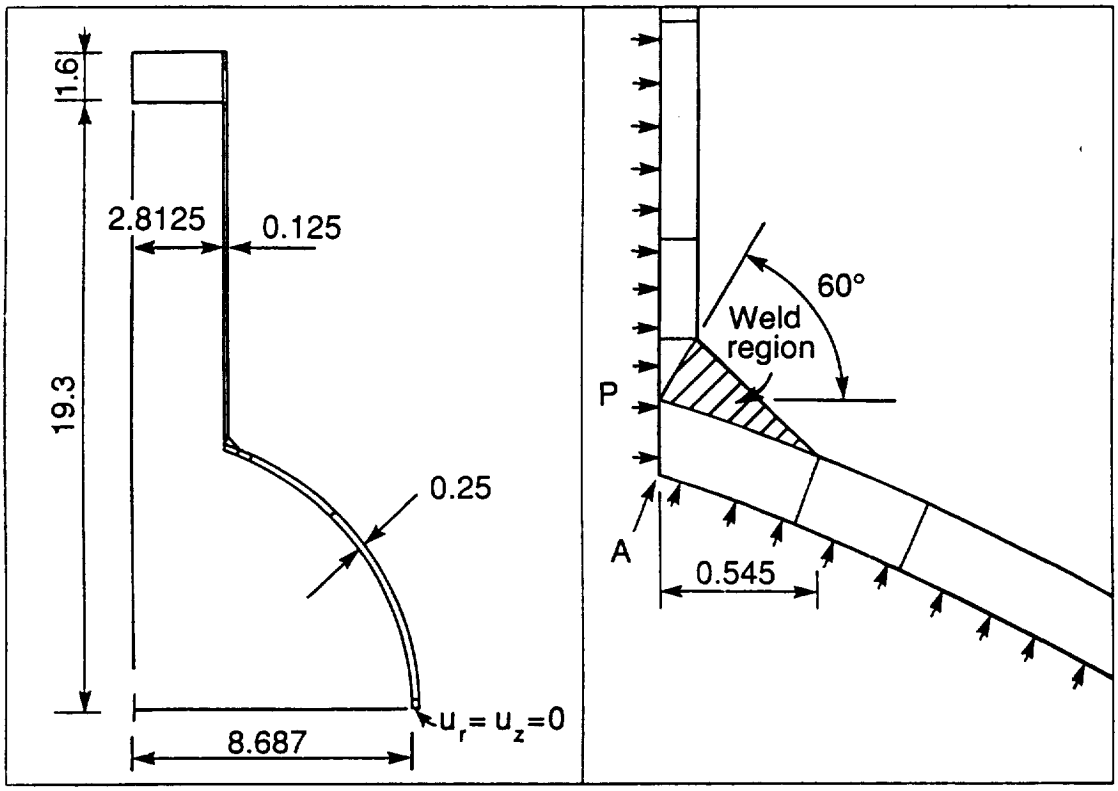

Fig. 7. Spherical pressure vessel. Generating section and mesh.

Uniform pressure $(T_n = -p,\ T_t = 0)$ was imposed on the inner surface of the vessel. The external surface was stress free $(T_n = T_t = 0)$. The displacement constraints $(u_r = u_z = 0)$ are indicated in Fig. 7.

The objectives of the analysis were to determine the vertical displacement of point A (u_z^A) for a range of pressure values which cause the vessel to yield extensively and to determine the size and shape of the resulting plastic zone.

A sequence of linear solutions was obtained by p-extension using the trunk space. The estimated relative error in energy norm of the finite element solution

Table 5. Results for the pressure vessel (Example 3).

Pressure (psi)	Displ. u_z^A (in)
760	7.02×10^{-3}
900	8.51×10^{-3}
1000	10.78×10^{-3}
1080	15.34×10^{-3}
1120	19.66×10^{-3}
1140	22.45×10^{-3}
1160	27.91×10^{-3}
1180	35.65×10^{-3}
1200	51.44×10^{-3}

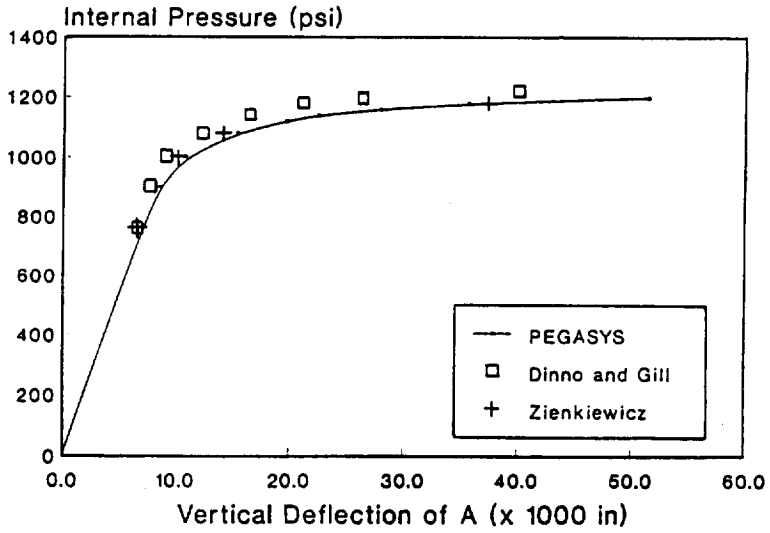

Fig. 8. Example 3: Internal pressure vs. axial displacement u_z^A.

at polynomial degree of 8 (trunk space), was 1.0 percent. There were 1056 degrees of freedom. The nonlinear analysis was performed at p-level 8 with the stopping criterion $\tau_\epsilon = 0.01$ (see eq. (12)). The results of the analysis for various values of the internal pressure are presented in Table 5 and in Fig. 8 which also includes the experimental and the finite elements results given in [12]. It is worth noting that the plastic zone spreads over the entire section of the nozzle-sphere intersection for values of $p \geq 900$ psi (see Fig. 9). Good agreement with the experimental results was obtained even for high values of pressure. The boundaries of the plastic zone for various values of the applied pressure are shown in Fig. 9. These results are substantially the same as those presented in reference [13].

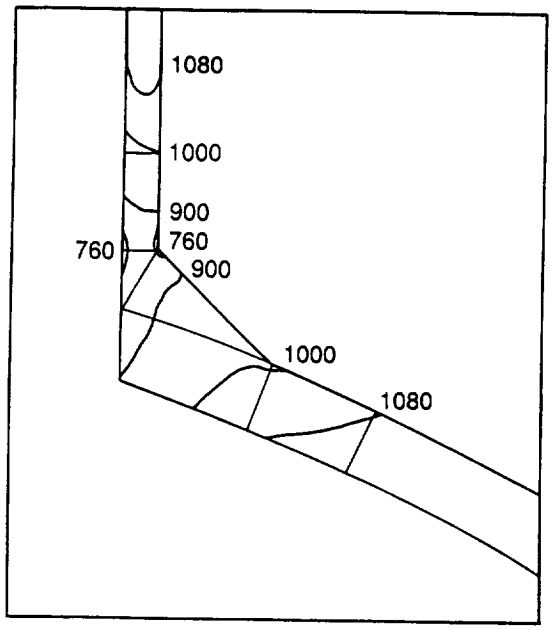

Fig. 9. Example 3: Boundaries of the plastic zone for various pressure values.

Example 4: Limit load in the case of plane strain.

In reference [5] Nagtegaal, Parks and Rice observed that finite element solutions based on the displacement formulation exhibit much too stiff response in the fully plastic range. Consequently, finite element solutions often exceed the limit load by substantial amounts and in some cases have no limit load at all. This is because plastic deformation occurs at a constant volume. In h-extensions based on the displacement formulation the constant volume constraints grow at the same or comparable rate as the number of degrees of freedom, hence locking occurs. This point is discussed in some detail in [6] also. Locking does not occur in p-extensions, however [6], [14]. The following example demonstrates that the formulation described in this paper will give the correct limit load when p-extension is used.

The most challenging example presented in reference [5] is the computation of the limit load for a deep double-edge-notch (DEN) plane strain tensile specimen. The example is challenging because the crack is very deep, the ligament is only $1/9th$ of the crack size, hence the crack tip singularity is strong.

The solution domain is shown in Fig. 10. The boundary conditions are as follows: On segments AB and EA symmetry conditions are prescribed ($u_n = T_t = 0$); on segment BC uniform normal displacement is imposed ($u_n = \delta/2$, $T_t = 0$);

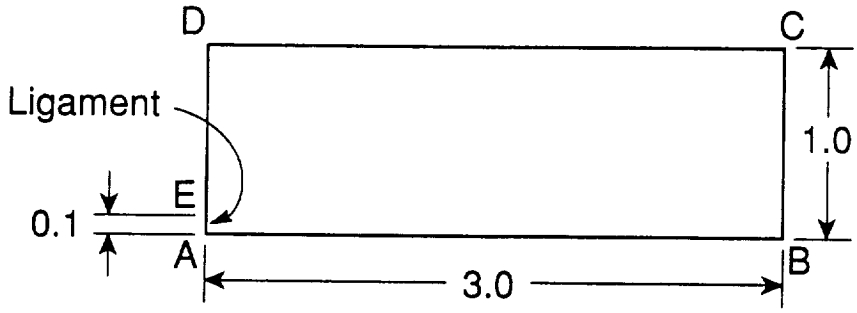

Fig. 10. Solution domain. Example 4.

segments CD and DE are stress free ($T_n = T_t = 0$). The modulus of elasticity and Poisson's ratio were 1.0 and 0.3 respectively, the yield stress was 1.0 also.

The finite element mesh was graded in geometric progression toward the singular point using the grading factor of 0.15. In addition, the mesh quality was checked by plotting the stress contours in the course of the nonlinear computations. The smoothness of the stress contours across interelement boundaries is an indicator of mesh quality. With the exception of the final load case, the trunk space at $p = 8$ was used. The number of degrees of freedom was 2143. In the final load case the product space was used at $p = 8$. The corresponding number of degrees of freedom was 4183.

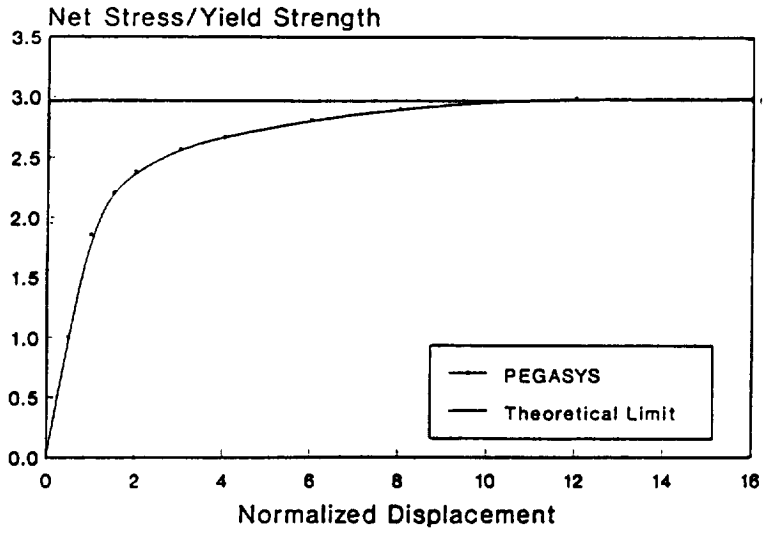

Fig. 11. Example 4. Normalized average stress vs. normalized displacement.

For the von Mises yield condition the limit load in terms of the net stress on the ligament is given by $\sigma_{lim} = (2 + \pi)\sigma_Y/\sqrt{3} \approx 2.97\sigma_Y$. The normalized stress (i.e.,

the average stress on the ligament divided by σ_Y is plotted against the normalized displacement in Fig. 11. The normalized displacement is defined by $E\delta/(\sigma_Y w)$ where w is the width of the strip (in this example $w = 2.0$). It is seen that the theoretical limit load is reached at high values of the imposed displacement.

SUMMARY AND CONCLUSIONS

The deformation theory of plasticity is a useful model of elastic-plastic behavior under certain restrictive assumptions which were described in this paper.

On comparing the deformation theory with the incremental theory in a carefully controlled numerical experiment, Example 1, it was found that the differences are smaller than errors in physical experiments designed to test alternative hypotheses concerning elastic-plastic constitutive relationships and the natural variations in elastic-plastic material properties. In this experiment the plastic zone was completely confined by an elastic zone and the exact solution was smooth.

The other examples point to the same conclusion: In the numerical experiments described under Examples 2 to 4 the accuracy of the reference solutions was not known, nevertheless it can be said that the results obtained by means of the deformation theory were within a few percent of results reported by other investigators based on the incremental theory.

While of course general conclusions from a few experiments would not be warranted, the results are consistent with those obtained by Hodge and White [1] and with Budiansky's observation that "deformation theories of plasticity may be used for a range of loading paths other than proportional loading without violation of the general soundness of a plasticity theory" [2]. In fact, the differences are so small that physical experiments could not distinguish between the deformation theory and the incremental theories of plasticity in any of the examples discussed in this paper.

The formulation of the elastic-plastic problem described in this paper is based on the displacement method. This is possible because p-extensions are not susceptible to Poisson ratio locking. The correct limit loads are obtained.

It has been demonstrated for the deformation theory of plasticity that p-extensions are effective for controlling errors of discretization associated with elastic-plastic material behavior. Similar results have been obtained for the incremental theory even in cases where unloading resulted in reverse plasticity [15].

REFERENCES

[1] Hodge, P. G., Jr. and White, G. N., Jr., "A Quantitative Comparison of Flow and Deformation Theories of Plasticity", *Journal of Applied Mechanics*, Vol. 17, pp. 180-184 (1950).

[2] Budiansky, B., "A Reassessment of Deformation Theory of Plasticity", *Journal of Applied Mechanics*, Trans. Am. Soc. Mech. Engrs, Vol. 81E, pp. 259-264 (1959).

[3] Rice, J. R., "A Path Independent Integral and the Approximate Analysis of Strain Concentration by Notches and Cracks", *Journal of Applied Mechanics*, Trans. Am. Soc. Mech. Engrs, Vol. 35, pp. 379-386 (1968).

[4] Hutchinson, J. W., "Singular Behavior at the End of a Tensile Crack in a Hardening Material", *J. Mech. Phys. Solids*, Vol. 16, pp. 13-31 (1968).

[5] Nagtegaal, J. C., Parks, D. M. and Rice, J. R., "On Numerically Accurate Finite Element Solutions in the Fully Plastic Range", *Computer Methods in Applied Mechanics and Engineering*, Vol. 4, pp. 153-177 (1974).

[6] Szabó, B. and Babuška, I., *Finite Element Analysis*, John Wiley & Sons Inc., New York (1991).

[7] Oden, J. T., "Smart Algorithms and Adaptive Methods in Computational Fluid Dynamics", Proc. 12th Canadian Congress of Applied Mechanics, May 28-June 2, 1989.

[8] Holzer, S. M., "Das symmetrische Randelementverfahren: Numerische Realisierung und Kopplung mit der Finite-Elemente-Methode zur elastoplastischen Strukturanalyse", Doctoral dissertation, Technische Universität München (1992).

[9] Galin, L. A., "Plane Elastic-Plastic Problem Plastic Zones in the Vicinity of Circular Apertures", (in Russian) *Prikladnaya Matematika i Mekanika*, Vol. X, pp. 367-386 (1946).

[10] Annin, B. D. and Cherepanov, G. P., *Elastic-Plastic Problems*, ASME Press, New York (1988).

[11] Theocaris, P. S. and Marketos, E. "Elastic-Plastic Analysis of Perforated Thin Strips of a Strain-Hardening Material", *J. Mech. Phys. Solids*, Vol. 12, pp. 377-390, 1964.

[12] Dinno, K. S. and Gill, S. S., "An Experimental Investigation into the Plastic Behaviour of Flush Nozzles in Spherical Pressure Vessels", *Int. J. Mech. Sci.*, Vol. 7, pp. 817-839, 1965.

[13] Zienkiewicz, O. C., "The Finite Element Method", McGraw Hill Company (UK) Limited, 1977.

[14] Szabó, B., A., Babuška, I. and Chayapathy, B. K., "Stress Computations for Nearly Incompressible Materials by the p-Version of the Finite Element Method", *Int. J. for Numerical Methods in Engineering* Vol. 28, pp. 3175-2190 (1989).

[15] Holzer, S. M. and Yosibash, Z., "The p-Version of the Finite Element Method in Incremental Elasto-plastic Analysis", Technical Report WU/CCM-93/4, Center for Computational Mechanics, Washington University, St. Louis, MO 63130.